Theory Guide: CFDEMcouplingPU

Jari Kolehmainen, Xiaoyu Liu, Ali Ozel, and Sankaran Sundaresan

September 22, 2022

1 Fluid Phase

The fluid phase momentum equation is given by [15] [16],

$$\frac{\partial(\alpha_f \rho_f \tilde{v}_{f,j})}{\partial t}+\frac{\partial(\alpha_f \rho_f \tilde{v}_{f,j}\tilde{v}_{f,i})}{\partial x_i} = -\alpha_f \frac{\partial \tilde{P}}{\partial x_j}+\frac{\partial(\alpha_f \tilde{\tau}_{ij})}{\partial x_i}-\frac{\partial(\alpha_f \tau_{ij}^{\alpha})}{\partial x_i}+\sum_p \beta_{f,p}[\tilde{v}_{f@p,j}-v_{p,j}] \tag{1}$$

where α_f is fluid volume fraction, ρ_f is the fluid density and $\tilde{v}_{f,i}$ is the filtered fluid velocity. $\tilde{v}_{f@p,j}$ is the undisturbed fluid velocity at the location of particle j. $\tilde{\tau}_{ij}$ is the filtered stress and is generally expressed as

$$\tilde{\tau}_{ij} = \mu_f(\alpha_f)[\frac{\partial \tilde{v}_{f,i}}{\partial x_j}+\frac{\partial \tilde{v}_{f,j}}{\partial x_i}] \tag{2}$$

where $\mu_F(\alpha_f)$ is taken to be simply μ_f of fluid as a default. This approximation fails at higher and higher particle loading.

τ_{ij}^{α} is the subgrid scale stress and is given as [13]

$$\tau_{ij}^{\alpha} = -2\mu_{SGS}\tilde{S}_{ij}+\frac{1}{3}\tau_{kk}\delta ij \tag{3}$$

where $\tilde{S}_{ij} = \frac{1}{2}[\frac{\partial \tilde{v}_{f,i}}{\partial x_j}+\frac{\partial \tilde{v}_{f,j}}{\partial x_i}]$. μ_{SGS} is the subgrid scale viscosity, which can be estimated as,

$$\mu_{SGS} = \rho_f(C_{SGS}\Delta)^2\sqrt{2\tilde{S}_{ij}\tilde{S}_{ij}} \tag{4}$$

where C_{SGS} is the Smagorinsky constant given by Dynamic Germano-Lilly model [5] [10],

$$C_{SGS} = \frac{1}{2}\frac{L_{ij}M_{ij}}{M_{ij}M_{ij}} \tag{5}$$

where

$$M_{ij} = \widehat{\Delta}^2\sqrt{2\widehat{\tilde{S}}_{ij}\widehat{\tilde{S}}_{ij}\widehat{\tilde{S}}_{ij}} - \Delta^2\sqrt{2\tilde{S}_{ij}\tilde{S}_{ij}\tilde{S}_{ij}} \tag{6}$$

$$L_{ij} = \rho_f(\widehat{\tilde{v}_{f,i}\tilde{v}_{f,j}} - \widehat{\tilde{v}}_{f,i}\widehat{\tilde{v}}_{f,j}) \tag{7}$$

where $\widehat{\ }$ is the test filtered quantity with filter size $\hat{\Delta}$.

2 Particle Phase

In the Discrete Element Method [2], particle motion is tracked by solving Newton's equations of motion:

$$m_i\frac{d\boldsymbol{v}_i}{dt} = \sum_j(\boldsymbol{f}^n_{c,ij}+\boldsymbol{f}^t_{c,ij})+\sum_k \boldsymbol{f}_{v,ik}+\sum_w(\boldsymbol{f}^n_{c,iw}+\boldsymbol{f}^t_{c,iw}+\boldsymbol{f}_{v,iw})+\boldsymbol{f}_{e,i}+\boldsymbol{f}_{g\to p,i}+m_i\boldsymbol{g} \tag{8}$$

$$I_i\frac{d\boldsymbol{\omega}_i}{dt} = \sum_j \boldsymbol{T}_{t,ij} + \sum_w \boldsymbol{T}_{t,iw} \tag{9}$$

In the equations, particle i has mass m_i, moment of inertia I_i, translational and angular velocities $\boldsymbol{v}_i$ and $\boldsymbol{\omega}_i$. The forces acting on the particle i are: $\boldsymbol{f}^n_{c,ij}$ and $\boldsymbol{f}^t_{c,ij}$ which are the normal and tangential contact forces between two particles i and j; $\boldsymbol{f}^n_{c,iw}$ and $\boldsymbol{f}^t_{c,iw}$, the normal and tangential contact forces between particle i and a wall; $\boldsymbol{f}^n_{v,ik}$ and $\boldsymbol{f}^t_{v,iw}$, the van der Waals forces from the interactions between particle i and k and particle i and a wall; $\boldsymbol{f}_{e,i}$, the electrostatic force on particle i; $\boldsymbol{f}_{g\to p,i}$, the total interaction force on the particle i due to surrounding gas modeled by the Wen and Yu drag law, and $m_i\boldsymbol{g}$, the gravitational force. The torque acting on particle i due to particle j is $\boldsymbol{T}_{t,ij}$. $\boldsymbol{T}_{t,ij} = \boldsymbol{R}_{ij}\times\boldsymbol{f}^t_{c,ij}$, where $\boldsymbol{R}_{ij}$ is the vector from the center of particle i to the contact point. $\boldsymbol{T}_{t,iw}$ is the torque acting on particle i from wall.

2.1 Contact Forces

The particle contact forces $\boldsymbol{f}^n_{c,ij}$ and $\boldsymbol{f}^t_{c,ij}$ are calculated by the following [9, 3]:

$$\boldsymbol{f}^n_{c,ij} = \frac{4}{3}Y^*\sqrt{r^*}\delta_n^{3/2}\boldsymbol{n}_{ij} + 2\sqrt{\frac{5}{6}}\beta\sqrt{S_n m^*}\boldsymbol{v}^n_{ij}, \tag{10}$$

$$\boldsymbol{f}^t_{c,ij} = \begin{cases} -8G^*\sqrt{r^*\delta_n}\boldsymbol{t}_{ij} - 2\sqrt{\frac{5}{6}}\beta\sqrt{S_t m^*}\boldsymbol{v}^t_{ij} & for \quad \left|\boldsymbol{f}^t_{c,ij}\right| < \mu_s\left|\boldsymbol{f}^n_{c,ij}\right| \\ -\mu_s\left|\boldsymbol{f}^n_{c,ij}\right|\frac{\boldsymbol{t}_{ij}}{|\boldsymbol{t}_{ij}|} & for \quad \left|\boldsymbol{f}^t_{c,ij}\right| \geq \mu_s\left|\boldsymbol{f}^n_{c,ij}\right|, \end{cases} \tag{11}$$

where

$$\frac{1}{Y^*} = \frac{1-\nu_i^2}{Y_i} + \frac{1-\nu_j^2}{Y_j}, \quad \frac{1}{r^*} = \frac{1}{r_i} + \frac{1}{r_j}, \tag{12}$$

$$\beta = \frac{ln(e)}{\sqrt{ln^2(e)+\pi^2}}, \quad S_n = 2Y^*\sqrt{r^*\delta_n}, \tag{13}$$

$$\frac{1}{G^*} = \frac{2(2+\nu_i)(1-\nu_i)}{Y_i} + \frac{2(2+\nu_j)(1-\nu_j)}{Y_j}, \quad S_t = 8G^*\sqrt{r^*\delta_n}. \tag{14}$$

The subscripts i, j denote spherical particle i or j, and the superscript $*$ denotes the effective particle property of those two particles. The effective particle mass m^* is calculated as $m^* = m_i m_j/(m_i+m_j)$; δ_n is normal overlap distance; $\boldsymbol{n}_{ij}$ represents the unit normal vector pointing from particle j to particle i; $\boldsymbol{v}^n_{ij}$ represents the normal velocity of particle j relative to particle i; $\boldsymbol{t}_{ij}$ represents the tangential displacement obtained from the integration of the relative tangential velocity during the contact, $\boldsymbol{v}^t_{ij}$; and μ_s is the particle sliding friction coefficient. Here, Y is Young's modulus, G is shear modulus, ν is Poisson's ratio, and r is particle radius. Eqns. (10) and (11) for the Hertzian contact model can be used to model particle contact forces between a particle and a wall $\boldsymbol{f}^n_{c,iw}$ and $\boldsymbol{f}^t_{c,iw}$ as well. The only difference is that particle j is now treated as a particle with infinite radius, and thus $m^* = m_i$.

2.2 Van der Waals Forces

The magnitude of van der Waals force F_{vdw} between particles i and k is modelled by the following [4] [8],

$$F_{vdw}(A,s) = \frac{A}{3}\frac{2r_i r_j(r_i+r_k+s)}{s^2(2r_i+2r_k+s)^2}\left[\frac{s(2r_i+2r_k+s)}{(r_i+r_k+s)^2-(r_i-r_k)^2} - 1\right]^2 \tag{15}$$

where A is the Hamaker constant, and s is the distance between the particle surfaces. It is assumed that the force saturates at a minimum separation distance, s_{min} (corresponding to the inter-molecular spacing). A maximum cutoff distance $s_{max} = (r_i + r_j)/r_i r_j$ is used to accelerate the simulation. For $s > s_{max}$, the van der Waals froce is not accounted for. The van der Waals force $\boldsymbol{f}_{v,ik}$ between particles i and k can be modeled as [7],

$$\boldsymbol{f}_{v,ik} = -f_{v,ik}\boldsymbol{n}_{ik} = \begin{cases} -F_{vdw}(A,s)\boldsymbol{n}_{ik} & for \quad s_{min} < s < s_{max} \\ -F_{vdw}(A,s_{min})\boldsymbol{n}_{ik} & for \quad s \leq s_{min} \end{cases} \tag{16}$$

The van der Waals force $\boldsymbol{f}_{v,iw}$ between particles i and wall experienced by particle i can be modeled as [7],

$$\boldsymbol{f}_{v,iw} = -f_{v,iw}\boldsymbol{n}_{iw} = \begin{cases} -\frac{Ar_i}{6s^2}\boldsymbol{n}_{iw} & for \quad s_{min} < s < s_{max} \\ -\frac{Ar_i}{6s_{min}^2}\boldsymbol{n}_{iw} & for \quad s \leq s_{min} \end{cases} \tag{17}$$

2.3 Softening Correction

Discrete Element Method (DEM) simulations of particles resolve collisional contact between particles. The higher the Youngs modulus of the particles, the smaller the time step must be. It is common in DEM simulations to artificially lower the Youngs modulus to speed up computations. This softening is known to affect predictions when interparticle forces are present; thus a number of softening corrections have been included so as to ensure that the softened simulations yield results that are close to the real system.

For normal contacts, the modified cohesion force $\boldsymbol{f}^M_{v,ik}$ between particles i and k can be modeled as

$$\boldsymbol{f}^M_{v,ik} = -f^M_{v,ik}\boldsymbol{n}_{ik} = \begin{cases} -F_{vdw}(A^R, s - s_0)\boldsymbol{n}_{ik} & for \quad s^S_{min} < s < s_{max} \\ -F_{vdw}(A^S, s^R_{min})\boldsymbol{n}_{ik} & for \quad s \leq s^S_{min} \end{cases} \tag{18}$$

and the modified cohesion force $\boldsymbol{f}^M_{v,iw}$ between particle i and wall experienced by particle i can be modeled as

$$\boldsymbol{f}^M_{v,iw} = -f^M_{v,iw}\boldsymbol{n}_{iw} = \begin{cases} -\frac{A^R r_i}{6(s-s_0)^2}\boldsymbol{n}_{iw} & for \quad s^S_{min} < s < s_{max} \\ -\frac{A^S r_i}{6{s^R_{min}}^2}\boldsymbol{n}_{iw} & for \quad s \leq s^S_{min} \end{cases} \tag{19}$$

Here, A^S is calculated by $A^S = A^R\theta$, where A^R is the original Hamaker constant; Y_S and Y_R are Young's moduli of softened system and real system respectively; $\theta = (Y_S/Y_R)^{0.4}$ for Hertzian contact model. s_0 and s^S_{min} are additional model parameters, which can be calculated by solving the following equations.

$$F_{vdw}(\theta, S^R_{min}) = F_{vdw}(1, s^S_{min} - s_0) \tag{20}$$

$$F_{vdw}(1, s^R_{min})\cdot s^R_{min} + \int_{s^R_{min}}^{s_{max}} F_{vdw}(1, s)ds = F_{vdw}(\theta, s^R_{min})\cdot S^S_{min} + \int_{s^S_{min}}^{s_{max}} F_{vdw}(1, s - s_0)ds \tag{21}$$

Details about the above model can be found in [7].

For tangential contacts, the sliding friction coefficient for a softened system, μ^S_s, can be obtained from $\mu^S_s = \mu^R_s/\theta$, where μ^R_s is the sliding friction coefficient of the real system and $\theta = (Y_S/Y_R)^{0.4}$ for Hertzian contact model[17, 1]. The rolling friction coefficient for a softened system, μ^S_r, can be obtained from $\mu^S_r = \mu^R_r/\theta$, where μ^R_r is the rolling friction coefficient of the real system[17, 1].

2.4 Turbulent Dispersion

The fluid-particle force for particle i can be expressed as

$$F^i_d = \beta(U^*_g - U_{p,i}) \tag{22}$$

where U^*_g is the gas phase velocity seen by particle i, $U_{p,i}$ the velocity of particle i, β the interfacial drag coefficient. U^*_g can be decomposed into two components as follow,

$$U^*_g = U_g + u^*_g \tag{23}$$

where U_g is the resolved gas phase velocity interpolated to particle location and u^*_g is the subgrid-scale (SGS) stochastic velocity that is experienced by each particle due to turbulence dispersion.

The SGS stochastic velocity seen by the particle can be modeled by the Langevin equation[14].

$$du^*_{g,i} = -\frac{u^*_{g,i}}{\tau^*_{sgs}}dt + \sqrt{\frac{2\sigma^2_{sg}}{\tau^*_{sgs}}}dW_i \tag{24}$$

where $u^*_{g,i}$ is the ith component of u^*_g. τ^*_{sgs} is the subgrid time scale of the fluid seen, given by

$$\tau^*_{sgs} = \frac{C_L k_{sgs}}{\epsilon} \tag{25}$$

The model constant C_L can be given by

$$C_L = (\frac{1}{2} + \frac{3}{4}C_0)^{-1} \tag{26}$$

where $C_0 \approx 2.1$[6]. ϵ, the energy dissipation rate, can be given by

$$\epsilon = (\nu_g + \nu_e)|S| \tag{27}$$

where ν_g is the gas-phase viscosity, $|S|$ the shear rate. ν_e is the eddy viscosity given by

$$\nu_e = (C_s\Delta)^2|S| \tag{28}$$

where Δ is the filter size. $C_s \approx 0.08$.

σ_{sg} is the subgrid velocity scale of the fluid seen, given by

$$\sigma_{sg} = \sqrt{\frac{2}{3}k_{sgs}} \tag{29}$$

where k_{sgs}, subgrid kinetic energy, is given by

$$k_{sgs} = 5C_s^2\Delta^2S^2 \tag{30}$$

dW_i is an increment of the Wiener process in ith component. The first order Euler discretization of Equation 24 gives

$$u_i^{*(t+1)} = au_i^{*(t)} + b\xi \tag{31}$$

where $u_i^{*(t+1)}$ at the next time step depends on $u_i^{*(t)}$ at the previous time step plus a stochastic contribution $\xi \sim N(0,1)$. a and b can be expressed as

$$a = e^{-\frac{\Delta t}{\tau^*_{sgs}}} \tag{32}$$

$$b = \sigma_{sg}\sqrt{1-a^2} \tag{33}$$

where Δt is the step size.

2.5 Electrostatic Forces

The electric force $\boldsymbol{f}_{e,i}$ on particle i has two physical contributions: Coulombic interactions and dielectrophoretic forces. Coulombic forces will depend on

the particle charge q_i, while dielectrophoretic forces are dependent on the particle's electric dipole $\boldsymbol{p}_i$. These forces can be modelled as

$$\boldsymbol{f}_{e,i} = q_i \boldsymbol{E}(\boldsymbol{x}_i) + \boldsymbol{p}_i \cdot \nabla \boldsymbol{E}(\boldsymbol{x}_i), \tag{34}$$

where $\boldsymbol{E}(\boldsymbol{x}_i)$ is the electric field at the particle position. Electric field is obtained by superposition of individual particles electric fields in conjunction with contributions coming from boundary conditions. Electric field emitted by a single particle at position $\boldsymbol{x}_i$ is

$$\boldsymbol{E}_i(\boldsymbol{x}) \;=\; \frac{q}{4\pi\varepsilon_0 r^2}\boldsymbol{n} + \frac{3(\boldsymbol{n}\cdot\boldsymbol{p}_i)\boldsymbol{n} - \boldsymbol{p}_i}{4\pi\varepsilon_0 r^3}, \tag{35}$$

where $r = \|\boldsymbol{x} - \boldsymbol{x}_i\|$ and $\boldsymbol{n} = (\boldsymbol{x} - \boldsymbol{x}_i)/r$.

To evaluate the electric field directly from all the particles at all the particle positions requires $O(N^2)$ evaluations for N particles, which is computationally very costly. If the system has conducting or insulating boundaries, the computations become even more costly as electric field needs to be evaluated at the surface patches to compute the surface charge densities. For this reason, one can evaluate the electric field at the grid scale by solving a Poisson equation for electric potential defined by $\boldsymbol{E} = -\nabla\phi$, where ϕ is the electric potential. Maxwell equations for static problem (particles moving with a velocity much lower than the speed of light) for electrical potential simplify to

$$\varepsilon_0 \nabla^2 \phi = -\rho_q + \nabla \cdot \boldsymbol{P}, \tag{36}$$

where $\boldsymbol{P}$ is the dipole density (or polarization density) and charge density is obtained by

$$\rho_q(\boldsymbol{x}) = \sum_i^N q_i \delta(\boldsymbol{x} - \boldsymbol{x}_i)). \tag{37}$$

The mesh method based on the Poisson equation will require very fine mesh (below particle diameter) to resolve the rapidly varying field near particles, and is therefore impractical. In the next sections, we will describe a particle-particle particle-mesh (P3M) approach that combines the two. This method will be based on modifying the charge density (and dipole densities) by adding and subtracting a Gaussian cloud:

$$\rho_q(\boldsymbol{x}) \;=\; \sum_i^N (q_i\left(\delta(\boldsymbol{x} - \boldsymbol{x}_i)\right) - G_i(\boldsymbol{x})) + q_i G_i(\boldsymbol{x})) \tag{38}$$

$$\;=\; \rho_q^s(\boldsymbol{x}) + \rho_q^l(\boldsymbol{x}), \tag{39}$$

where $\rho_q^s(\boldsymbol{x})$ is the short-range contribution of the charge density, $\rho_q^l(\boldsymbol{x}) = \sum_i^N q_i G_i(\boldsymbol{x})$ is the contribution due to the charges carried by all the particles. $G_i(\boldsymbol{x})$ is Gaussian distribution centered around particle i:

$$G_i(\boldsymbol{x}) = \frac{1}{(\sqrt{2\pi}\sigma)^3} \exp\left(-\frac{r^2}{2\sigma^2}\right), \tag{40}$$

where σ is known as the Ewald parameter and has the unit of distance. Now the electric field contribution from $\rho_q^s(\boldsymbol{x})$ will be rapidly decaying and can be handled by direct summation over neighbors, while the contribution from $\rho_q^l(\boldsymbol{x})$ is smoothly varying and can be captured with mesh larger than a particle.

2.5.1 Short-Range Coulombic Interactions

To evaluate the short-distance contribution, we need explicit forms for the electric potential, electric field, and the gradient of electric field. Electric potential for particle i represented as a point charge subtracted by the Gaussian cloud is obtained by the following integral:

$$\begin{aligned} \phi_i^{s,q}(\boldsymbol{x}) &= q_i \int_{\mathbb{R}^3} \frac{\delta(\boldsymbol{y} - \boldsymbol{x}_i)) - G_i(\boldsymbol{y})}{4\pi\varepsilon_0 r_y} d\boldsymbol{y} && (41) \\ &= \frac{q_i \operatorname{erfc}(\frac{r}{\sqrt{2}\sigma})}{4\pi\varepsilon_0 r}. && (42) \end{aligned}$$

Electric field is obtained by taking gradient and becomes:

$$\begin{aligned} \boldsymbol{E}_i^{s,q}(\boldsymbol{x}) &= -\nabla\phi_i^{s,q}(\boldsymbol{x}) && (43) \\ &= q_i \boldsymbol{n} \left(\frac{\operatorname{erfc}(\frac{r}{\sqrt{2}\sigma})}{4\pi\varepsilon_0 r^2} + \frac{\sqrt{\frac{2}{\pi}} \exp(-\frac{r^2}{2\sigma^2})}{4\pi\varepsilon_0 \sigma r} \right). && (44) \end{aligned}$$

Finally, gradient of electric field is given by:

$$\begin{aligned} \nabla \boldsymbol{E}_i^{s,q}(\boldsymbol{x}) &= q_i (\mathrm{I} - \boldsymbol{n} \otimes \boldsymbol{n}) \left(\frac{\operatorname{erfc}(\frac{r}{\sqrt{2}\sigma})}{4\pi\varepsilon_0 r^3} + \frac{\sqrt{\frac{2}{\pi}} \exp(-\frac{r^2}{2\sigma^2})}{4\pi\varepsilon_0 \sigma r^2} \right) && (45) \\ &\quad - q_i \, \boldsymbol{n} \otimes \boldsymbol{n} \left(\frac{\sqrt{\frac{2}{\pi}} e^{-\frac{r^2}{2\sigma^2}}}{2\pi\varepsilon_0 \sigma r^2} + \frac{\sqrt{\frac{2}{\pi}} e^{-\frac{r^2}{2\sigma^2}}}{4\pi\varepsilon_0 \sigma^3} + \frac{\operatorname{erfc}(\frac{r}{\sqrt{2}\sigma})}{2\pi\varepsilon_0 r^3} \right). && (46) \end{aligned}$$

2.5.2 Short-Range Dielectrophoretic Interactions

We will follow the same decomposition for the polarization density:

$$\boldsymbol{P}(\boldsymbol{x}) = \sum_i^N \boldsymbol{p}_i \left(\delta(\boldsymbol{x} - \boldsymbol{x}_i)) - G_i(\boldsymbol{x})\right) + \boldsymbol{p}_i G_i(\boldsymbol{x}) = \boldsymbol{P}^s(\boldsymbol{x}) + \boldsymbol{P}^l(\boldsymbol{x}). \quad (47)$$

To evaluate the interactions from the first part ($\boldsymbol{P}^s(\boldsymbol{x})$), we need an expression for electric potential, electric field, and electric field gradient from point source subtracted by the Gaussian cloud. This can be obtained by following integral:

$$\begin{aligned}
\phi_i^{s,p}(\boldsymbol{x}) &= -\boldsymbol{p}_i \cdot \nabla \left(\int_{\mathbb{R}^3} \frac{\delta(\boldsymbol{y} - \boldsymbol{x}_i)) - G_i(\boldsymbol{y})}{4\pi\varepsilon_0 r_y} d\boldsymbol{y} \right) && (48)\\
&= -\boldsymbol{p}_i \cdot \nabla \left(\frac{\operatorname{erfc}(\frac{r}{\sqrt{2}\sigma})}{4\pi\varepsilon_0 r} \right) && (49)\\
&= (\boldsymbol{p}_i \cdot \boldsymbol{n}) \left(\frac{\operatorname{erfc}(\frac{r}{\sqrt{2}\sigma})}{4\pi\varepsilon_0 r^2} + \frac{\sqrt{\frac{2}{\pi}} \exp(-\frac{r^2}{2\sigma^2})}{4\pi\varepsilon_0 \sigma r} \right) && (50)
\end{aligned}$$

with $r_y = \|\boldsymbol{y} - \boldsymbol{x}_i\|$. Electric field spanned by the potential can be found by taking a gradient:

$$\begin{aligned}
\boldsymbol{E}_i^{s,p}(\boldsymbol{x}) &= -\nabla \phi_i^s(\boldsymbol{x}) && (51)\\
&= -((\boldsymbol{p}_i \cdot \boldsymbol{n})\boldsymbol{n} - \boldsymbol{p}_i) \left(\frac{\operatorname{erfc}(\frac{r}{\sqrt{2}\sigma})}{4\pi\varepsilon_0 r^3} + \frac{\sqrt{\frac{2}{\pi}} \exp(-\frac{r^2}{2\sigma^2})}{4\pi\varepsilon_0 \sigma r^2} \right) && (52)\\
&\quad + (\boldsymbol{p}_i \cdot \boldsymbol{n})\boldsymbol{n} \left(\frac{\sqrt{\frac{2}{\pi}} e^{-\frac{r^2}{2\sigma^2}}}{2\pi\varepsilon_0 \sigma r^2} + \frac{\sqrt{\frac{2}{\pi}} e^{-\frac{r^2}{2\sigma^2}}}{4\pi\varepsilon_0 \sigma^3} + \frac{\operatorname{erfc}(\frac{r}{\sqrt{2}\sigma})}{2\pi\varepsilon_0 r^3} \right) && (53)\\
&= -\boldsymbol{p}_i \cdot (\boldsymbol{n} \otimes \boldsymbol{n} - \mathrm{I}) \left(\frac{\operatorname{erfc}(\frac{r}{\sqrt{2}\sigma})}{4\pi\varepsilon_0 r^3} + \frac{\sqrt{\frac{2}{\pi}} \exp(-\frac{r^2}{2\sigma^2})}{4\pi\varepsilon_0 \sigma r^2} \right) && (54)\\
&\quad + \boldsymbol{p}_i \cdot \boldsymbol{n} \otimes \boldsymbol{n} \left(\frac{\sqrt{\frac{2}{\pi}} e^{-\frac{r^2}{2\sigma^2}}}{2\pi\varepsilon_0 \sigma r^2} + \frac{\sqrt{\frac{2}{\pi}} e^{-\frac{r^2}{2\sigma^2}}}{4\pi\varepsilon_0 \sigma^3} + \frac{\operatorname{erfc}(\frac{r}{\sqrt{2}\sigma})}{2\pi\varepsilon_0 r^3} \right) && (55)
\end{aligned}$$

To estimate the short-range dielectrophoretic forces, one also requires expression for the gradient of the short-range electric field $\nabla \boldsymbol{E}_i^{s,p}(\boldsymbol{x})$. This gradient of the electric field can be evaluated as:

$$\nabla \boldsymbol{E}_i^{s,p}(\boldsymbol{x}) = \mathrm{P}_{\nabla}^{s} \left(\frac{\operatorname{erfc}(\frac{r}{\sqrt{2}\sigma})}{4\pi\varepsilon_0 r^3} + \frac{\sqrt{\frac{2}{\pi}} e^{-\frac{r^2}{2\sigma^2}}}{4\pi\varepsilon_0 \sigma^3} + \frac{\sqrt{\frac{2}{\pi}} e^{-\frac{r^2}{2\sigma^2}}}{4\pi\varepsilon_0 \sigma r^2} \right) \tag{56}$$

$$- \boldsymbol{p}_i \otimes \boldsymbol{n} \left(\frac{3\operatorname{erfc}(\frac{r}{\sqrt{2}\sigma})}{4\pi\varepsilon_0 r^4} + \frac{3\sqrt{\frac{2}{\pi}} e^{-\frac{r^2}{2\sigma^2}}}{4\pi\varepsilon_0 \sigma r^3} + \frac{\sqrt{\frac{2}{\pi}} e^{-\frac{r^2}{2\sigma^2}}}{4\pi\varepsilon_0 \sigma^3 r} \right) \tag{57}$$

$$- (\boldsymbol{p}_i \cdot \boldsymbol{n}) \boldsymbol{n} \otimes \boldsymbol{n} \left(\frac{3\operatorname{erfc}(\frac{r}{\sqrt{2}\sigma})}{4\pi\varepsilon_0 r^4} + \frac{3\sqrt{\frac{2}{\pi}} e^{-\frac{r^2}{2\sigma^2}}}{4\pi\varepsilon_0 \sigma r^3} + \frac{\sqrt{\frac{2}{\pi}} e^{-\frac{r^2}{2\sigma^2}}}{4\pi\varepsilon_0 \sigma^3 r} \right) \tag{58}$$

$$- (\boldsymbol{p}_i \cdot \boldsymbol{n}) \boldsymbol{n} \otimes \boldsymbol{n} \left(\frac{3\sqrt{\frac{2}{\pi}} e^{-\frac{r^2}{2\sigma^2}}}{4\pi\varepsilon_0 \sigma^4} + \frac{\sqrt{\frac{2}{\pi}} r e^{-\frac{r^2}{2\sigma^2}}}{4\pi\varepsilon_0 \sigma^5} \right), \tag{59}$$

where tensor P_{∇}^{s} is given by following expression

$$\mathrm{P}_{\nabla}^{s} = \nabla \left((\boldsymbol{p}_i \cdot \boldsymbol{n}) \boldsymbol{n} \right) \tag{60}$$

$$= \frac{\boldsymbol{p}_i \cdot \boldsymbol{n}}{r} \mathrm{I} + \frac{\boldsymbol{p}_i \otimes \boldsymbol{n}}{r} - \frac{2(\boldsymbol{p}_i \cdot \boldsymbol{n})}{r} \boldsymbol{n} \otimes \boldsymbol{n}. \tag{61}$$

2.5.3 Long-Range Interactions

We solve Poisson equation for long range electric potential in a mesh

$$\varepsilon_0 \nabla^2 \phi^l(\boldsymbol{x}) = -\rho_q^l(\boldsymbol{x}) + \nabla \cdot \boldsymbol{P}^l(\boldsymbol{x}), \tag{62}$$

where the long-range densities are given by

$$\rho_q^l(\boldsymbol{x}) = \sum_i q_i G_i(\boldsymbol{x}) \tag{63}$$

$$\boldsymbol{P}^l(\boldsymbol{x}) = \sum_i \boldsymbol{p}_i G_i(\boldsymbol{x}). \tag{64}$$

Electric field and its gradient can be obtained from the long-range potential $\phi^l(\boldsymbol{x})$ by taking gradients numerically at the mesh-level. Furthermore,

particles will not reside in the mesh centers, and an interpolation scheme is required to map the mesh values into the particle positions.

2.5.4 Electric Field and Force Computations

To obtain electric field and the gradient at the location of particle i, we need to combine the various terms:

$$\boldsymbol{E}(\boldsymbol{x}_i) = -\nabla\phi^l(\boldsymbol{x}_i) + \sum_{0<\|\boldsymbol{x}_j-\boldsymbol{x}_i\|<r_c} \boldsymbol{E}_j^{s,q}(\boldsymbol{x}_i) + \boldsymbol{E}_j^{s,p}(\boldsymbol{x}_i) \tag{65}$$

$$\nabla\boldsymbol{E}(\boldsymbol{x}_i) = -(\nabla\otimes\nabla)\phi^l(\boldsymbol{x}_i) + \sum_{0<\|\boldsymbol{x}_j-\boldsymbol{x}_i\|<r_c} \nabla\boldsymbol{E}_j^{s,q}(\boldsymbol{x}_i) + \nabla\boldsymbol{E}_j^{s,p}(\boldsymbol{x}_i), \tag{66}$$

where r_c is cut-off radius that essentially depends on the Ewald parameter. For large Ewald parameters, the short-range interaction terms decay slower and the cut-off radius needs to be larger for smaller Ewald parameters. Typically, the cut-off radius will be a few particle diameters. Once, the electric field and the gradient are known, particle forces can be evaluated according to Eq. (34).

2.5.5 Polarization

For insulating materials, the electric dipole is not an independent constant, but rather a function of the electric field itself. For linear isotropic dielectric materials the polarization density is connected to electric field by

$$\boldsymbol{P} = \chi\varepsilon_0\boldsymbol{E}, \tag{67}$$

with susceptibility χ, which is a material property. The resulting electric dipole is obtained by integration

$$\boldsymbol{p}_i = \int_{V_{p,i}} \boldsymbol{P}d\boldsymbol{y} \tag{68}$$

$$= \alpha_p\varepsilon_0 V_p\boldsymbol{E}, \tag{69}$$

where α_p is known as the polarizability of the particle. Polarizability is connected to the susceptibility by Clausius-Mossotti relation:

$$\alpha_p = 3\frac{\chi}{\chi+2}. \tag{70}$$

Since electric field depends on the electric dipoles, determining the polarization of the particles becomes an n-body problem. For a small number of particles, this can be solved directly by Gaussian elimination, but that is not an option for larger numbers of particles due to the computational cost of $O(N^3)$. Furthermore, the resulting matrix will be dense and the memory requirement will scale as $O(N^2)$. To avoid the direct solution, we will solve the problem with Jacobi iterations that reads:

$$\boldsymbol{p}_i^{(n)} = \alpha_p \varepsilon_0 V_{p,i} \boldsymbol{E}_i^{(n-1)}, \tag{71}$$

where (n) refers to the iteration index and $\boldsymbol{E}_i^{(0)}$ is obtained from the Coulombic interactions (both short-range and long-range interactions included). This iterative scheme converges in a few iterations for most practical problems.

Another remaining issue is that each Jacobi iteration will now require solution of the Poisson equation, since $\boldsymbol{P}^l$ is changing. To avoid this, we will estimate the long-range polarization density using a long-range mixture permittivity. This approach decouples the long-range computations from the particle scale computations.

Before proceeding we define short-hand for spatial averaging:

$$\alpha_s(\boldsymbol{x})\tilde{h}(\boldsymbol{x}) \;=\; \sum_i V_{p,i} h_i G_i(\boldsymbol{x}) \tag{72}$$

with volume fraction defines as

$$\alpha_s(\boldsymbol{x}) \equiv \sum_i V_{p,i} G_i(\boldsymbol{x}). \tag{73}$$

We decompose the polarization density into two parts as follows:

$$\begin{aligned}
\boldsymbol{P}^l(\boldsymbol{x}) &= \sum_i \boldsymbol{p}_i G_i(\boldsymbol{x}) && (74)\\
&= \sum_i \alpha_p \varepsilon_0 V_{p,i} G_i(\boldsymbol{x}) \boldsymbol{E}_i && (75)\\
&= \sum_i \alpha_p \varepsilon_0 V_{p,i} G_i(\boldsymbol{x}) \left(-\nabla \phi^l(\boldsymbol{x}_i) + \sum_{j \neq i} \boldsymbol{E}_j^{s,q}(\boldsymbol{x}_i) + \boldsymbol{E}_j^{s,p}(\boldsymbol{x}_i) \right) && (76)\\
&= -\sum_i \alpha_p \varepsilon_0 V_{p,i} \nabla \phi^l(\boldsymbol{x}_i) G_i(\boldsymbol{x}) && (77)\\
&\quad + \sum_i \alpha_p \varepsilon_0 V_{p,i} G_i(\boldsymbol{x}) \sum_{j \neq i} \left(\boldsymbol{E}_j^{s,q}(\boldsymbol{x}_i) + \boldsymbol{E}_j^{s,p}(\boldsymbol{x}_i) \right). && (78)
\end{aligned}$$

The first term can be expressed using the previously defined spatial average in Eq. (72):

$$\sum_i \alpha_p \varepsilon_0 V_{p,i} \nabla \phi^l(\boldsymbol{x}_i) G_i(\boldsymbol{x}) = \alpha_p \varepsilon_0 \alpha_s(\boldsymbol{x}) \nabla \tilde{\phi}^l(\boldsymbol{x}). \tag{79}$$

For simplicity we will neglect the short-range effects on the long-range polarization density. This will allow us to write:

$$\boldsymbol{P}^l(\boldsymbol{x}) = -\alpha_p \varepsilon_0 \alpha_s(\boldsymbol{x}) \nabla \tilde{\phi}^l(\boldsymbol{x}) \approx -\varepsilon_0 \alpha_p \alpha_s(\boldsymbol{x}) \nabla \phi^l(\boldsymbol{x}). \tag{80}$$

Inserting to the Poisson equation will produce:

$$\nabla \cdot \left(\varepsilon_m^l \nabla \phi^l \right) = -\frac{\rho_q^l}{\varepsilon_0} \tag{81}$$

with mixture permittivity

$$\varepsilon_m^l = 1 + \alpha_p \alpha_s(\boldsymbol{x}). \tag{82}$$

3 Coarse Grained API Transport Model

In a typical DPI application, the total number of particles can be several tens of millions. For example, a full simulation of the experiment in Nguyen et al.[12] would require tracking over 80 million particles. Such systems require impractically large computational resources. Thus, van Wachem et al.[16] and Nguyen et al.[12] adopted an Eulerian-coarsening approach where API particles are modeled as passive scalars. We have outlined this approach in this section for reader's reference. This model is **currently NOT implemented** in the code. Instead, we decided to follow an Euler-Lagrangian coarsening approach, which is outlined in the next section.

In this approach, one can treat the API particle concentration as continuous concentration field, c_p, which is defined as the number density of API particles suspended in the fluid. We also assume that the API particles carry a charge q_p. The transport equation for the API particle concentration will become:

$$\frac{\partial \alpha_f c_p}{\partial t} + \nabla \cdot (\alpha_f \tilde{\boldsymbol{v}}_f c_p) = \nabla \cdot (\alpha_f \kappa_{fp} \nabla c_s) + I_{c \to s} - \nabla \cdot (\sigma_c \alpha_f c_p \boldsymbol{E}), \tag{83}$$

where $I_{c\to s}$ is API particle transfer from carrier particles to the fluid due to carrier particle collisions, or due to API particle attachment/detachment; κ_{fp} is API particle dispersion coefficient; σ_c is API particle electric mobility.

The mobility term σ_c can be closed by analyzing API particle force balance. If one neglects API particle inertia, the electrostatic force on API particles immersed in the fluid will be balanced by the fluid drag (Stoke's drag assumed here due to small particle size):

$$q_p \boldsymbol{E} = 3\pi\mu_f d_{api} \boldsymbol{u}_{\text{slip}}, \tag{84}$$

where μ_f is the fluid dynamic viscosity; d_{api} is API particle diameter; and $\boldsymbol{u}_{\text{slip}}$ is the difference between the API particle velocity and the fluid velocity. Hence, the particle flux due to the electric field becomes:

$$\alpha_f c_p \boldsymbol{u}_{\text{slip}} = \left(\frac{q_p}{3\pi\mu_f d_{api}} \right) \alpha_f c_p \boldsymbol{E}, \tag{85}$$

which allows us to identify that the mobility is given by following expression:

$$\sigma_c = \frac{q_p}{3\pi\mu_f d_{api}}. \tag{86}$$

Following van Wachem [16], the API particle transfer can be divided to four sub-terms:

$$I_{c\to s} = I^{pp}_{c\to s} + I^{pw}_{c\to s} + I^{\text{f}}_{c\to s} + I^{rc}_{c\to s}, \tag{87}$$

where $I^{pp}_{c\to s}$ is detachment of API particles due to carrier particle collisions; $I^{pw}_{c\to s}$ is detachment of API particles due to carrier particle collisions with the wall; $I^{\text{f}}_{c\to s}$ detachment of API particles due to fluid flow; $I^{rc}_{c\to s}$ is reattachment of API particles from the fluid flow. The following discussion neglects the electrostatic effects on the API particles, and only takes into account Van der Waals forces between API and carrier particles.

The first term $I^{pp}_{c\to s}$ is expressed by

$$I^{pp}_{c\to s} = \frac{1}{V_{\text{cell}}\Delta t} \sum_i I_{pp,i}, \tag{88}$$

where V_{cell} is the cell volume; Δt is the fluid time interval where collisions took place; summation is taken over all the carrier particles in the cell; $I_{pp,i}$ is the number of API particles released during the time step from carrier

particle i due to particle-particle collisions. The second term $I^{pw}_{c\to s}$ is given by

$$I^{pw}_{c\to s} = \frac{1}{V_{\text{cell}}\Delta t}\sum_i I_{pw,i}, \tag{89}$$

where $I_{pw,i}$ is the API particles released from carrier particle i (and wall) due to particle-wall collisions during the fluid time step. It should be noted that we lump the API particles released from the wall to the carrier particle release and do not treat the wall particles as separate source.

The release due to collisions is modeled as

$$I_{pp,i} = \frac{1}{2}\sum_j \eta^{pp}_{ij}\left(A_{p,i}c_{p,i} + A_{p,j}c_{p,j}\right) \tag{90}$$

$$I_{pw,i} = \frac{1}{2}\sum_j \eta^{pw}_{ij}\left(A_{p,i}c_{p,i} + A_{p,j}c_{p,j}\right), \tag{91}$$

where summation is over all the collisions that took place during the time interval; j is the index of the particle or wall element; $A_{p,i}$ is the surface area of carrier particle i or surface area of the wall element. The coefficients η^{pp}_{ij} and η^{pw}_{ij} are given by

$$\eta^{p*}_{ij} = \begin{cases} B^{p*}_0 U^{B^{p*}_1}_{n,ij} & \text{if } U_{n,ij} < B_2 \\ B^{p*}_3 U^{B^{p*}_4}_{n,ij} & \text{otherwise.} \end{cases} \tag{92}$$

Here $U_{n,ij}$ refers to relative normal velocity between the particles or particle and a wall; the symbol $*$ may refer to either particles or wall, and the B^{p*}_i $(i = 1, 2, 3, 4)$ are empirical parameters that depend on the Hameker constant.

Detachment of particles due to fluid flow ($I^{\text{f}}_{c\to s}$) is modeled as

$$I^{\text{f}}_{c\to s} = \frac{1}{V_{\text{cell}}}\sum_i I_{f,i}, \tag{93}$$

where the $I_{f,i}$ stands for the number of particles detached from the carrier particle i per unit time and is expressed as

$$I_{f,i} = E_0 \max(\|\boldsymbol{v}_{p,i} - \tilde{\boldsymbol{v}}_{f@p,i}\| - U_0, 0)^{E_1} A_{p,i}c_{p,i}, \tag{94}$$

where E_0, E_1, and U_0 are empirical coefficients; $A_{p,i}$ is the surface area of the carrier particle i; $c_{p,i}$ is the number of API particles per unit area of carrier

particle. Finally, the reattachment rate of fines to the carrier particles per unit volume is given by

$$I_{c\to s}^{\mathrm{rc}} = -\sum_i I_{rc,i}, \tag{95}$$

where $I_{rc,i}$ is the number of API particles reattached to the carrier particle i per unit time. Carrier particle reattachment rate is given by

$$I_{rc,i} = A_{p,i}\alpha_{f@p}c_{s@p}\|\boldsymbol{v}_{p,i} - \tilde{\boldsymbol{v}}_{f@p,i}\|, \tag{96}$$

$c_{s@p}$ is the API particle concentration in the fluid interpolated to the carrier particle location. The last part $\|\boldsymbol{v}_{p,i} - \tilde{\boldsymbol{v}}_{f@p,i}\|$ assumes that the API particles are moving with the fluid velocity. If electrostatic forces are present, the API particle velocity might differ from the fluid velocity and the expression would require modification.

To formulate a boundary condition for the API particles, we assume that the wall has a surface API particle density c_w. Near the boundary, we assume that API particles deposit at the wall with rate proportional to c_p. Particles already adhered at the wall are detached by fluid shear. The total flux of API particles from the wall (API particles per unit time per unit area) will be modeled as:

$$\theta(c_s) = \mathcal{A}\alpha_f c_p \boldsymbol{n}_w - \mathcal{B}c_w\boldsymbol{n}_w, \tag{97}$$

where $\mathcal{A}$ and $\mathcal{B}$ are parameters that depend on the level of cohesion, shear-rate and other factors; $\boldsymbol{n}_w$ is the wall outward normal vector.

Equating the flux at the wall to the interior flux from the wall ($-\alpha_f\kappa_{fp}\nabla c_s + \sigma_c\alpha_f c_p\boldsymbol{E}$) and taking dot product with the wall outward normal leads to:

$$(\mathcal{A} - \sigma_c\boldsymbol{E}\cdot\boldsymbol{n}_w)\alpha_f c_p - \mathcal{B}c_w + \alpha_f\kappa_{fp}\frac{\partial c_p}{\partial \boldsymbol{n}_w} = 0. \tag{98}$$

Boundary API particle surface density will then follow:

$$\frac{\partial c_w}{\partial t} = \mathcal{A}\alpha_f c_p - \mathcal{B}c_w. \tag{99}$$

4 Particle-based coarse-graining approach

Instead of treating API particles as passive scalars in the Eulerian-coarsening approach outlined in the previous section, we pursued a particle-based Lagrangian-coarsening approach, including the more conventional discrete Parcel approach and the representative particle approach, proposed in Liu et 2021 [11].

In order to reduce the number of entities tracked in the simulation, we propose the following representative particle approach. While still tracking all the carrier particles, we only track a representative subset of API particles, where each simulated API particle represents N primary API particles, and N is known as the coarsening factor. Essentially, we interpret each representative particle as N primary particles located in the same location, $\boldsymbol{x}$, and with the same velocity, $\boldsymbol{v}$.

The representative particle approach is different from the more conventional Discrete Parcel Method in the following aspects. In the Discrete Parcel Method, each parcel represents N primary particles, and in the context of DPI formulations, both the carrier and API particles would be coarse-grained in the same manner. In the representative particle approach, only API particles are coarse-grained, whereas all carrier particles are still tracked in the simulation. When resolving particle collisions, a parcel is treated as a bigger particle with an equivalent volume of N primary particles, whereas in the representative particle approach, particle sizes are the same as the original system. (When the Discrete Parcel Method is coupled with CFD, the fluid-particle interaction force is still computed using the primary particle diameter and multiplied by N to get the force on the parcel.) In the Discrete Parcel Method, both the number of carrier parcels and API parcels would be reduced to $1/N$ of those in the original system. In the representative particle approach, the number of carrier particles is the same as the original system, whereas the number of representative API particles is reduced to $1/N$ of that in the original system. These comparisons are summarized in Table 1 and illustrated in Figure 1. In the representative particle approach, API particle diameter remains the same after coarsening, as shown in Figure 1b.

In the representative particle approach, the DEM equation for carrier particles is as follows. N is the coarsening factor for API particles.

Table 1: Comparison between the Discrete Parcel Method approach and the representative particle approach. d is the diameter of a primary particle. N_c and N_{API} are the numbers of carrier and API particles, respectively in the original system. N is the coarsening factor.

	Discrete Parcel Method	Representative Particle Approach
Methodology	N primary particles $\rightarrow$ 1 parcel (for both carrier and API)	N primary API particles $\rightarrow$ 1 representative API particle
Particle diameter (in DEM)	$N^{1/3}d$	d
Number of carrier particles	N_c/N	N_c
Number of API particles	N_{API}/N	N_{API}/N

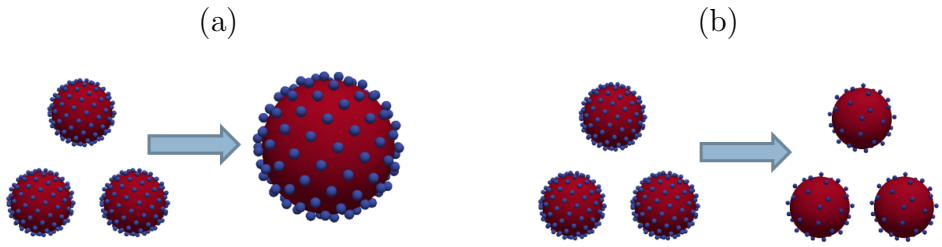

Figure 1: Schematic illustrations of a) the Discrete Parcel Method and b) the representative particle approach. The original system in this example consists of 3 carrier particles with a diameter of 70.0 and 387 API particles with a diameter of 5.0. After coarse-graining (with $N = 3$) using the Discrete Parcel Method in (a) and the representative particle approach in (b), the system consists of a) one carrier parcel with a diameter of 101.0 and 129 API parcels with a diameter of 7.2 and b) 3 carrier particles with a diameter of 70.0 and 129 representative API particles with a diameter of 5.0. In the rerpresentative particle approach, API particle diameter remains the same after coarse-graining.

$$m_i \frac{d\boldsymbol{v}_i}{dt} = \sum_j (\boldsymbol{f}^n_{c,ij} + \boldsymbol{f}^t_{c,ij}) + \sum_k (\boldsymbol{F}^n_{c,ik} + \boldsymbol{F}^t_{c,ik}) + \sum_p \boldsymbol{f}_{v,ip} + \sum_q \boldsymbol{F}_{v,iq} + \sum_w (\boldsymbol{f}^n_{c,iw} + \boldsymbol{f}^t_{c,iw} + \boldsymbol{f}_{v,iw}) + \boldsymbol{f}_{g\rightarrow p,i} + m_i \boldsymbol{g} \tag{100}$$

In this equation, m_i is the mass of carrier particle i. $\boldsymbol{v}_i$ is the translational velocity of carrier particle i. $\boldsymbol{f}^n_{c,ij}$ and $\boldsymbol{f}^t_{c,ij}$ are the normal and tangential contact forces between carrier particle i and carrier particle j. $\boldsymbol{F}^n_{c,ik}$ and $\boldsymbol{F}^t_{c,ik}$ are the normal and tangential contact forces between carrier particle i and representative API particle k. $\boldsymbol{F}^n_{c,ik} = N\boldsymbol{f}^n_{c,ik}$ and $\boldsymbol{F}^t_{c,ik} = N\boldsymbol{f}^t_{c,ik}$, where $\boldsymbol{f}^n_{c,ik}$ and $\boldsymbol{f}^t_{c,ik}$ are the normal and tangential contact forces between carrier particle i and one primary API particle at the same position as representative API particle k. The contact forces between carrier particle i and representative API particle k are equivalent to the contact forces between carrier particle i and N primary API particles.

$\boldsymbol{f}_{v,ip}$ is the van der Waals force between carrier particle i and carrier particle p. $\boldsymbol{F}_{v,iq}$ is the van der Waals force between carrier particle i and representative API particle q. $\boldsymbol{F}_{v,iq} = N\boldsymbol{f}_{v,iq}$, where $\boldsymbol{f}_{v,iq}$ is the van der Waals force between carrier particle i and one primary API particle at the same position as representative API particle q. Similarly, the van der Waals force between carrier particle i and representative API particle q is equivalent to that between carrier particle i and N primary API particles. $\boldsymbol{f}^n_{c,iw}$, $\boldsymbol{f}^t_{c,iw}$ and $\boldsymbol{f}_{v,iw}$ are the normal contact force, tangential contact force, and van der Waals force between carrier particle i and wall w. $\boldsymbol{f}_{g\to p,i}$ is the total force acting on carrier particle i by gas. $m_i\boldsymbol{g}$ is the gravitational force.

The DEM equation for representative API particles is as follows

$$M_i\frac{d\boldsymbol{v}_i}{dt} = \sum_j(\boldsymbol{F}^n_{c,ij} + \boldsymbol{F}^t_{c,ij}) + \sum_k(\boldsymbol{F}^n_{c,ik} + \boldsymbol{F}^t_{c,ik}) + \sum_p \boldsymbol{F}_{v,ip} + \sum_q \boldsymbol{F}_{v,iq} + \sum_w(\boldsymbol{F}^n_{c,iw} + \boldsymbol{F}^t_{c,iw} + \boldsymbol{F}_{v,iw}) + \boldsymbol{F}_{g\to p,i} + M_i\boldsymbol{g} \tag{101}$$

In this equation, M_i is the mass of representative API particle i, where $M_i = Nm_i$ as the mass of one representative API particle is equivalent to N primary API particles. $\boldsymbol{v}_i$ is the translational velocity of representative API particle i. $\boldsymbol{F}^n_{c,ij}$ and $\boldsymbol{F}^t_{c,ij}$ are the normal and tangential contact forces between representative API particle i and carrier particle j. $\boldsymbol{F}^n_{c,ij} = N\boldsymbol{f}^n_{c,ij}$ and $\boldsymbol{F}^t_{c,ij} = N\boldsymbol{f}^t_{c,ij}$, where $\boldsymbol{f}^n_{c,ij}$ and $\boldsymbol{f}^t_{c,ij}$ are the normal and tangential contact forces between carrier particle j and one primary API particle at the same position as representative API particle i, consistent with Eq. 100. $\boldsymbol{F}^n_{c,ik}$ and $\boldsymbol{F}^t_{c,ik}$ are the normal and tangential contact forces between representative

API particles i and k. $\boldsymbol{F}^n_{c,ik} = N\boldsymbol{f}^n_{c,ik}$ and $\boldsymbol{F}^t_{c,ik} = N\boldsymbol{f}^t_{c,ik}$, where $\boldsymbol{f}^n_{c,ik}$ and $\boldsymbol{f}^t_{c,ik}$ are the normal and tangential contact forces between two primary API particles which are at the same positions as representative API particles i and k, respectively. Since there are N on both sides of the equation, the contact forces between two representative API particles are equivalent to those between two primary API particles.

$\boldsymbol{F}_{v,ip}$ is the van der Waals force between representative API particle i and carrier particle p. $\boldsymbol{F}_{v,ip} = N\boldsymbol{f}_{v,ip}$, where $\boldsymbol{f}_{v,ip}$ is the van der Waals force between carrier particle p and one primary API particle at the same position as representative API particle i, consistent with Eq. 100. $\boldsymbol{F}_{v,iq}$ is the van der Waals force between representative API particles i and q. $\boldsymbol{F}_{v,iq} = N\boldsymbol{f}_{v,iq}$, where $\boldsymbol{f}_{v,iq}$ is the van der Waals force between two primary API particles, which are at the same positions as representative API particles i and q, respectively. Similar to contact forces, the van der Waals force between two representative API particles is equivalent to that between two primary API particles.

$\boldsymbol{F}^n_{c,iw}$, $\boldsymbol{F}^t_{c,iw}$ and $\boldsymbol{F}_{v,iw}$ are the normal contact force, tangential contact force and van der Waals force between representative API particle i and wall w. $\boldsymbol{F}^n_{c,iw} = N\boldsymbol{f}^n_{c,iw}$, $\boldsymbol{F}^t_{c,iw} = N\boldsymbol{f}^t_{c,iw}$ and $\boldsymbol{F}_{v,iw} = N\boldsymbol{f}_{v,iw}$, where $\boldsymbol{f}^n_{c,iw}$, $\boldsymbol{f}^t_{c,iw}$ and $\boldsymbol{f}_{v,iw}$ are the normal contact force, tangential contact force and van der Waals force between wall w and a primary API particle at the same position as representative API particle i. Thus, particle-wall interactions between one representative API particle and a wall are equivalent to those between N primary API particles and a wall. $\boldsymbol{F}_{g\to p,i}$ is the total force acting on representative API particle i. $\boldsymbol{F}_{g\to p,i} = N\boldsymbol{f}_{g\to p,i}$, where $\boldsymbol{f}_{g\to p,i}$ is the total force acting by gas on one primary API particle at the same position as representative API particle i. Since there are N on both sides of the DEM equation, the effect of total gas-particle interactions on one representative API particle is equivalent to that on one primary API particle. However, the effect of total gas-particle interactions by one representative API particle on gas is equivalent to that by N primary API particles.

References

[1] Sheng Chen, Wenwei Liu, and Shuiqing Li. A fast adhesive discrete element method for random packings of fine particles. *Chemical Engineering Science*, 193:336–345, 2019.

[2] Peter A Cundall and Otto DL Strack. A discrete numerical model for granular assemblies. *geotechnique*, 29(1):47–65, 1979.

[3] Alberto Di Renzo and Francesco Paolo Di Maio. Comparison of contact-force models for the simulation of collisions in dem-based granular flow codes. *Chemical engineering science*, 59(3):525–541, 2004.

[4] Janine E Galvin and Sofiane Benyahia. The effect of cohesive forces on the fluidization of aeratable powders. *AIChE Journal*, 60(2):473–484, 2014.

[5] Massimo Germano, Ugo Piomelli, Parviz Moin, and William H Cabot. A dynamic subgrid-scale eddy viscosity model. *Physics of Fluids A: Fluid Dynamics*, 3(7):1760–1765, 1991.

[6] Laurent YM Gicquel, P Givi, FA Jaberi, and SB Pope. Velocity filtered density function for large eddy simulation of turbulent flows. *Physics of Fluids*, 14(3):1196–1213, 2002.

[7] Yile Gu, Ali Ozel, and Sankaran Sundaresan. A modified cohesion model for cfd–dem simulations of fluidization. *Powder Technology*, 296:17–28, 2016.

[8] HC Hamaker. The londonvan der waals attraction between spherical particles. *physica*, 4(10):1058–1072, 1937.

[9] Kenneth Langstreth Johnson and Kenneth Langstreth Johnson. *Contact mechanics*. Cambridge university press, 1987.

[10] Douglas K Lilly. A proposed modification of the germano subgrid-scale closure method. *Physics of Fluids A: Fluid Dynamics*, 4(3):633–635, 1992.

[11] Xiaoyu Liu, Mostafa Sulaiman, Jari Kolehmainen, Ali Ozel, and Sankaran Sundaresan. Particle-based coarse-grained approach for simulating dry powder inhaler. *International Journal of Pharmaceutics*, 606:120821, 2021.

[12] Duy Nguyen, Johan Remmelgas, Ingela Niklasson Björn, Berend van Wachem, and Kyrre Thalberg. Towards quantitative prediction of the performance of dry powder inhalers by multi-scale simulations and experiments. *International journal of pharmaceutics*, 547(1-2):31–43, 2018.

[13] SB Pope. *Turbulent Flows, 6th ed.* Cambridge: Cambridge University Press, 2000.

[14] Jacek Pozorski and Sourabh V Apte. Filtered particle tracking in isotropic turbulence and stochastic modeling of subgrid-scale dispersion. *International Journal of Multiphase Flow*, 35(2):118–128, 2009.

[15] P Sagaut. *Large Eddy Simulation for Incompressible Flows, 3rd ed.* Springer, 2005.

[16] Berend van Wachem, Kyrre Thalberg, Johan Remmelgas, and Ingela Niklasson-Björn. Simulation of dry powder inhalers: Combining micro-scale, meso-scale and macro-scale modeling. *AIChE Journal*, 63(2):501–516, 2017.

[17] Kimiaki Washino, Ei L Chan, and Toshitsugu Tanaka. Dem with attraction forces using reduced particle stiffness. *Powder Technology*, 325:202–208, 2018.